| Frontiers in Chemistry

Electrical and magnetic properties of antiferromagnetic semiconductor $MnSi_2N_4$ monolayer

Dongke Chen[1,2], Zhengyu Jiang[2], Ying Tang[2], Junlei Zhou[2], Yuzhou Gu[2], Jing-Jing He[3] and Jiaren Yuan[1]*

[1]School of Physics and Materials Science Nanchang University, Nanchang, China, [2]School of Physics and Electronic Engineering, Jiangsu University, Zhenjiang, China, [3]College of Information Science and Technology, Nanjing Forestry University, Nanjing, China

Two-dimensional antiferromagnetic semiconductors have triggered significant attention due to their unique physical properties and broad application. Based on first-principles calculations, a novel two-dimensional (2D) antiferromagnetic material $MnSi_2N_4$ monolayer is predicted. The calculation results show that the two-dimensional $MnSi_2N_4$ prefers an antiferromagnetic state with a small band gap of 0.26 eV. $MnSi_2N_4$ has strong antiferromagnetic coupling which can be effectively tuned under strain. Interestingly, the $MnSi_2N_4$ monolayer exhibits a half-metallic ferromagnetic properties under an external magnetic field, in which the spin-up electronic state displays a metallic property, while the spin-down electronic state exhibits a semiconducting characteristic. Therefore, 100% spin polarization can be achieved. Two-dimensional $MnSi_2N_4$ monolayer has potential application in the field of high-density information storage and spintronic devices.

Introduction

In 2004, the successfully prepared graphene opened a new era of two-dimensional materials (Novoselov et al., 2004). Subsequently, numerous new systems have already been discovered, greatly promoting the development of the two-dimensional material family. Two-dimensional materials have a wide variety of electronic properties, including metallic, semi-metallic, semiconducting and insulating properties. For example, $1H$-MoS_2 is a semiconductor with a direct band gap, 1T phase MoS_2 is a metal, while 1T' phase MoS_2 is semimetal (Hung et al., 2018). In addition, hexagonal boron nitride (h-BN) shows insulating properties (Liu et al., 2003), and graphene is semimetal (Sheng et al., 2019). However, many 2D materials lack intrinsic magnetism, such as graphene and MoS_2, which motivates researchers to induce magnetism through defect engineering, adsorption or insertion of magnetic atoms. However, these schemes are difficult to construct stable

long-range magnetic order. Therefore, two-dimensional intrinsic ferromagnetic materials have aroused tremendous attention.

According to Mermin-Wagner theory, the long-range magnetic order is predicted to be unstable in 2D material and can be easily destroyed by thermal fluctuations (Mermin and Wagner, 1966). Until 2017, the magnetism in the two-dimensional material CrI_3 at the monolayer limit was observed experimentally (Gong et al., 2017; Huang et al., 2017). Hereafter, more 2D magnetic materials have been found, such as Fe_3GeTe_2 (Xian et al., 2022), $FePS_3$ (Lee et al., 2016) and VSe_2 (Bonilla et al., 2018). Two-dimensional magnetic materials possess a wide variety of excellent physical properties. For instance, monolayer magnetic metal materials have been widely used as electrodes in electronic devices, such as Fe_3GeTe_2 based van der Waals tunnel junctions (O'Hara et al., 2018). Furthermore, magnetic tunnel junction with antimagnetic semiconductor CrI_3 tunnel barrier has been reported to possess a giant magnetoresistance effect due to the significant difference of energy band in the ferromagnetic and antiferromagnetic states (Song et al., 2018), which has achieved a huge breakthrough in spintronic devices. Hence antiferromagnetic semiconductor materials have become a hot research topic because of their novel band characteristics. However, such materials are very rare, the prediction of new antiferromagnetic semiconductor materials becomes the key to the development of spintronic devices.

In this paper, the electronic structure and magnetic properties of monolayer $MnSi_2N_4$ are explored based on first-principles calculations. The results demonstrate that 2D $MnSi_2N_4$ is a stable antiferromagnetic semiconductor in which the ground state is an antiferromagnetic state. The large magnetic exchange parameter indicates a strong antiferromagnetic coupling between the magnetic Mn atoms. When an external magnetic field is applied, the $MnSi_2N_4$ monolayer turns into a half-metal with a magnetic state transition from an antiferromagnetic state to a ferromagnetic state. In which the spin-up electronic state displays a metallic nature, while the spin-down electronic state exhibits a semiconducting feature. Therefore, the $MnSi_2N_4$ monolayer has great application prospects in spintronics and nanosensors.

Computational details

All calculations were conducted using the Vienna *ab initio* simulation package (VASP) (Kresse and Furthmuller, 1996; Kresse and Joubert, 1999). The projection plane wave (PAW) method was adopted to describe the interaction between ions and electrons (Blöchl, 1994). The cutoff energy is set as 500 eV. The generalized gradient approximation (GGA) of the form

FIGURE 1
Top **(A)** and side **(B)** views of $MnSi_2N_4$. The balls are highlighted with blue (Si atom), purple (Mn atom) and silvery (N atom). The rhombic unit cells are marked with black dashed lines.
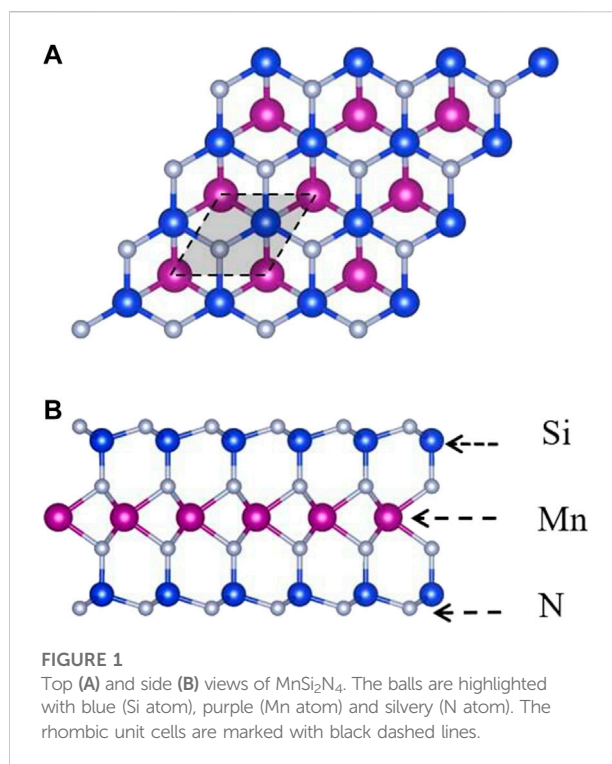
Perdew–Burke–Ernzerhof (PBE) was employed to describe the exchange correlation (Perdew et al., 1996). The convergence criteria for electronic iteration and ionic relaxation were 10^{-6} eV and 0.001 eV/Å, respectively. An 18 Å vacuum layer was added in the out plane direction of the monolayer $MnSi_2N_4$ to eliminate interlayer interactions. The Brillouin zone was sampled with a $13 \times 13 \times 1$ k-point mesh. Due to the strong correlation effect of Mn atoms, the DFT + U method proposed by Dudarev et al. (Dudarev et al., 1998) was adopted, and the effective parameter U_{eff} was set to 3.9 eV (Wang et al., 2006; Jain et al., 2011; Ling and Mizuno, 2012; Togo and Tanaka, 2015). The phonon spectrum of monolayer $MnSi_2N_4$ was calculated by the PHONONPY software (Togo et al., 2015) using a 5×5 supercell.

Results and discussion

Similar to the two-dimensional $MoSi_2N_4$, the monolayer $MnSi_2N_4$ is a two-dimensional material with a hexagonal lattice structure and D_{3h} point group as shown in Figure 1. $MnSi_2N_4$ monolayer consists of seven atomic layers stacked with the order N-Si-N-Mn-N-Si-N, which can be regarded as a 1H-phase MnN_2 triple-layer sandwiched between two buckled N-Si layers. The lattice constant of unit cell is 2.88Å, the bond length between Mn and N atoms is 2.02 Å and the bond length between Si and N atoms is 1.74 Å.

FIGURE 2
Phonon spectrum of monolayer $MnSi_2N_4$.
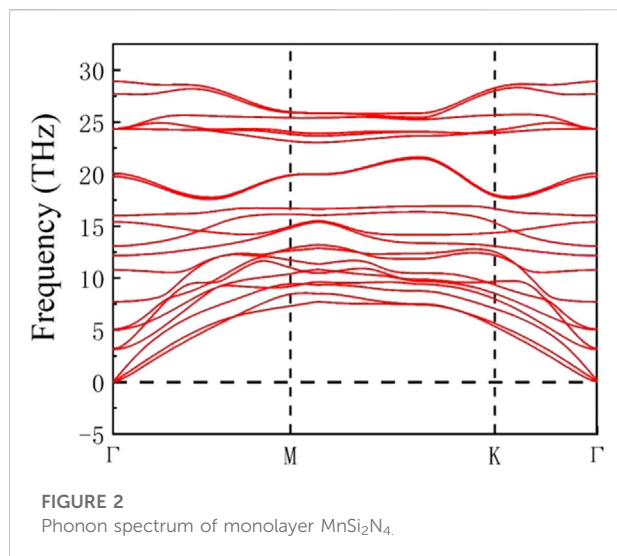
The cohesive energy of the monolayer $MnSi_2N_4$ was evaluated to confirm the stability of monolayer $MnSi_2N_4$ using the equation:

$$E_{coh} = (E_{MnSi_2N_4} - E_{Mn} - 2E_{Si} - 4E_N)/7 \qquad (1)$$

Where $E_{MnSi_2N_4}$ represents the energy of $MnSi_2N_4$, E_{Mn}, E_{Si} and E_N represent the energy of isolated single Mn, Si and N atoms, respectively. The calculated results show that the cohesive energy of $MnSi_2N_4$ is -5.03 eV/atom which is comparable to the value of

MoS_2 monolayer (−5.12 eV/atom) (Canton-Vitoria et al., 2020) and $MoSi_2N_4$ (−8.46 eV/atom) (Bafekry et al., 2021). We also calculated the phonon spectrum to check the stability, and there is no imaginary phonon frequency throughout the Brillouin zone, indicating that the structure is dynamically stable. Consequently, the $MnSi_2N_4$ monolayer has excellent stability and thus may be experimentally prepared in Figure 2.

The magnetic properties of monolayer $MnSi_2N_4$ were investigated. We first determined the ground-state magnetic ordering with two possible magnetic order ferromagnetic (FM) and antiferromagnetic (AFM) states. The total energies of the AFM and FM phases of $MnSi_2N_4$ are -218.650eV and -217.658 eV, respectively. The energy of the AFM state is lower than that of the FM state, hence $MnSi_2N_4$ has an AFM ground state. The AFM order in monolayer $MnSi_2N_4$ sourced from the superexchange interactions between two magnetic atoms bridged by nonmetal atoms, following the Goodenough-Kanamori rules (Goodenough, 1955; Kanamori, 1959). In this case, the net magnetic moment is zero and the four Mn atoms in the supercell have an antiparallel magnetic state along with the same value of magnetic moments (3.05 μ_B). The spin-polarized charge density and the schematic diagram for FM and AFM order are plotted in Figure 3. The spin-polarized charge density map shows that Mn atoms possess an high spin-polarized charge density, while spin-polariztion of N atoms is tiny with small magnetic moments (0.05 μ_B).

The electronic properties of AFM states are investigated to further explore potential applications of $MnSi_2N_4$. The electronic band structure and density of states (TDOS) are calculated as

FIGURE 3
(A,B) spin-polarized charge densities of the FM and AFM case for $MnSi_2N_4$. The yellow and light blue isosurface with an isosurface value of 0.05 e/Bohr^3 represent the spin-up and spin-down charge densities, respectively. **(C,D)** The scheme represents spin orientation of Mn atoms in FM and AFM case.
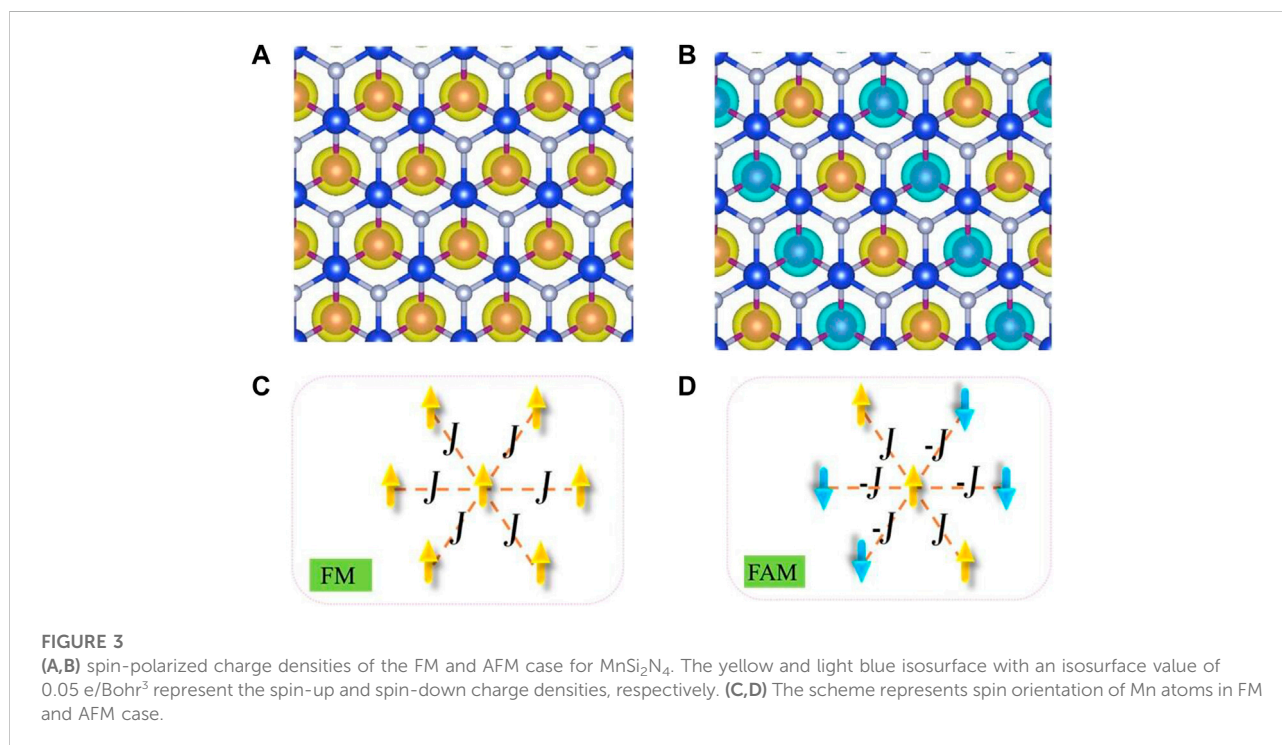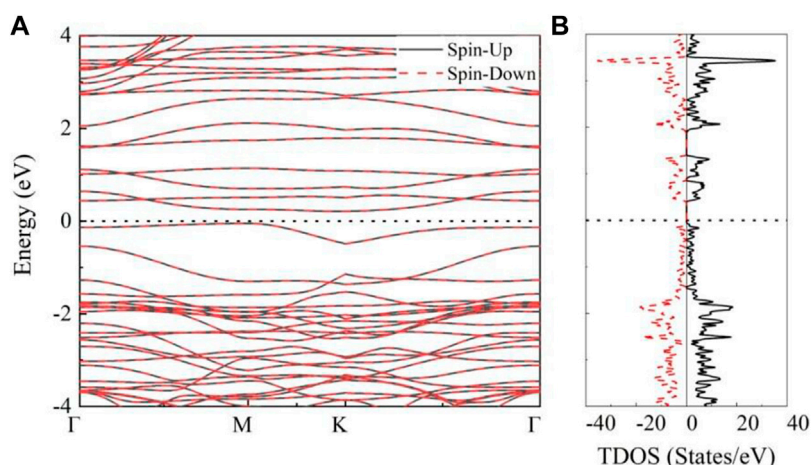
FIGURE 4
(A) The band structures and (B) total density of states (TDOS) of $MnSi_2N_4$ monolayer in the AFM states, the spin-up states and spin-down states are represented by the black lines and red dotted lines, respectively.
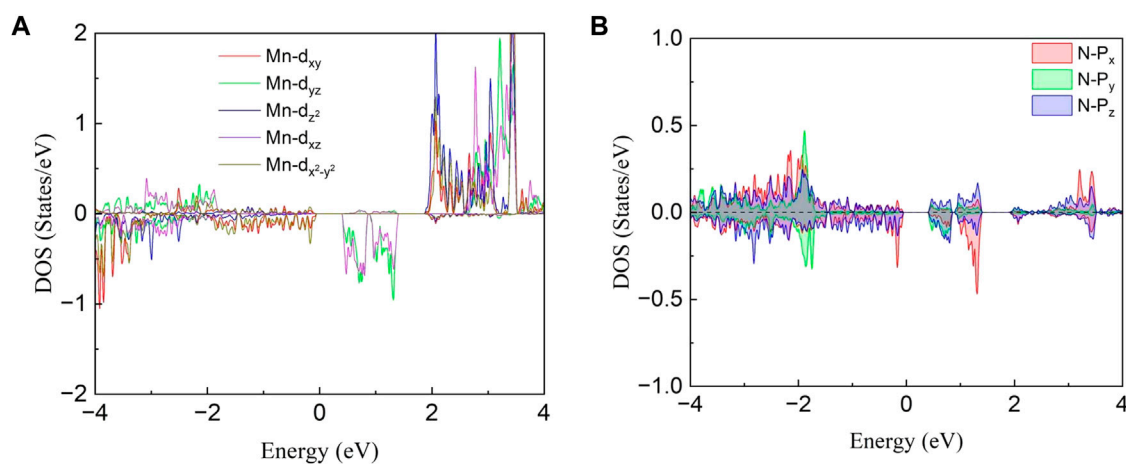
FIGURE 5
Projected density of states (PDOS) for (A) Mn-d orbital and (B) N-p orbital.

illustrated in Figure 4. It is clear that $MnSi_2N_4$ exhibits indirect semiconducting property without band cross Fermi level, which is different from nonmagnetic direct bandgap semiconductor $MoSi_2N_4$ monolayer (Yuan et al., 2022). The conduction band minimum (CBM) and the valence band maximum (VBM) are located at K point and M point, respectively. The band gap is small (0.26 eV). The bands are degenerate and the TDOS is symmetrical for spin-up and spin-down states. Furthermore, no states exist near the Fermi level along with a small energy gap.

The projected density of states (PDOS) for Mn atom and the nearest neighbor N atom are depicted in Figure 5 to better analyze orbit contribution for electron structure and magnetic properties. One can notice that the density of states for the five $3d$ orbitals are all asymmetric as shown in Figure 5A, indicating the large spin splitting for an isolated Mn atom. The magnetic moment (3.04 μ_B/Mn) is mainly dominated by the spin-up (majority-spin) states of d orbitals which is much more than the spin-down electron. For the N atom, the difference in PDOS between the spin-up and spin-down states is not obvious, resulting in a smaller magnetic moment. In addition, the DOS mainly comes from Mn-d and N-p in the energy range from 0.5 to 1.5 eV indicating that the hybridizations between the N-p and Mn-d orbitals are strong.
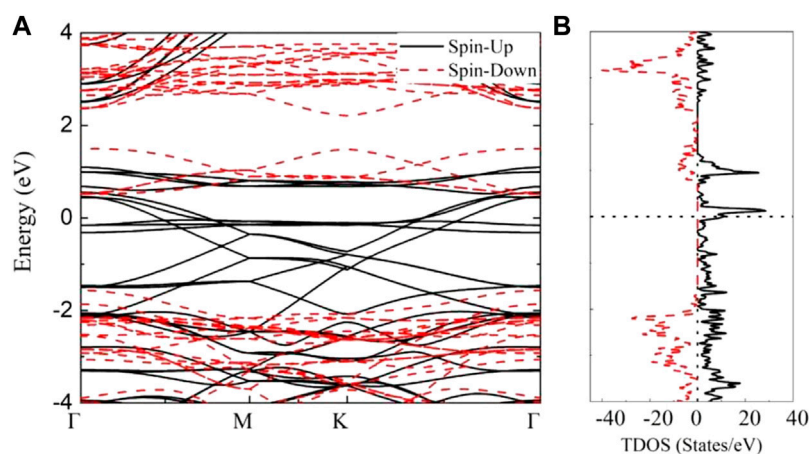
FIGURE 6
(A) The band structures and **(B)** total density of states (TDOS) of $MnSi_2N_4$ in the FM states, the spin-up states and spin-down states are represented by the black lines and red dotted lines, respectively.
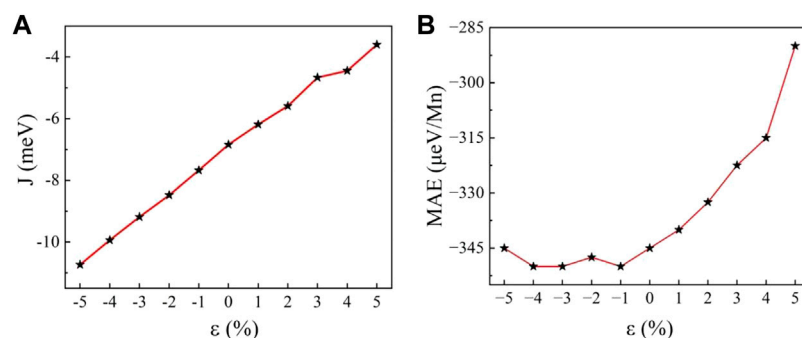
FIGURE 7
(A) Magnetic exchange parameter J and **(B)** magnetocrystalline anisotropy energy E_{MAE} as a function of strain.

Furthermore, the ground antiferromagnetic states will transition to ferromagnetic states under an external magnetic field. The band structure and density of states for FM state are depicted in Figure 6. It is clear that the spin-up and spin-down energy bands are not degenerate. The spin-polarized states can be noticed around the Fermi level. In the spin-up channel, several flat bands near the Fermi level existe and the others band display dispersion along Γ–M and K–Γ, which behave as a metal. But for the spin-down channel, a direct bandgap of 2.07 eV is observed with the VBM and CBM located at Γ point. Hence, $MnSi_2N_4$ monolayer behaves half-metallic properties in the FM case. The spin polarization is obvious with an asymmetric density of states distribution for spin-up and spin-down states as depicted in Figure 6B. One can find that a peak of spin-up

states can be seen near the Fermi level and a large bandgap exists in the spin-down states, which further confirms the metallic behavior for the spin-up states and semiconducting property for spin-down states, respectively. Therefore, the 2D $MnSi_2N_4$ in FM state is a half-metal with 100% spin polarization.

Strain is an effective means of manipulating electronic structure and magnetic properties which is widely utilized to modulate the electronic structure and magnetic properties of monolayer system. In this paper, the strain is defined as $\varepsilon = (a - a_0)/a_0$, where a_0 is the relaxed lattice constant in the equilibrium state. The magnetic moment of the Mn atom remains about 3 μ_B per unit cell under strain. The effective spin Hamiltonian based on the Heisenberg model can be expressed as

$$H = -\sum_{<i,j>} J_{ij}\mu_i\mu_j \qquad (2)$$

where J_{ij} is the magnetic exchange parameter, and μ_i/μ_j is the magnetic moment at nearest neighbor sites i and j, respectively (Kan et al., 2013). The magnetic exchange parameter J is a significant parameter, which can be evaluated by calculating the total energy of the system in different magnetic states. For the FM case, the total energy can be written as $E_{FM} = E_0 - 3 J | \mu |^2$, where E_0 represents the total energy without spin polarization. For the AFM case, the total energy can be expressed as $E_{AFM} = E_0 + J | \mu |^2$. Thus, the exchange parameter can be extracted by $J = (E_{AFM} - E_{FM})/4 | \mu |^2$. According to Figure 7A, although the value of J increases nearly linearly with biaxial strain, the energy difference between AFM case and FM case remains positive over the range of applied biaxial strain, indicating that $MnSi_2N_4$ behaves as AFM phase and no transition from AFM to FM phase is observed. Furthermore, the magnetic exchange parameter J increases with tensile strain and decreases with compressive strain. According to this trend, an extremely large tensile strain may be needed to turn the AFM to the FM ordering.

To identify the easy axis of $MnSi_2N_4$, we computed the magnetic anisotropy energy (MAE). The MAE of the magnetic crystal is defined as $E_{MAE} = E_{in}\text{-}E_{out}$ (Webster and Yan, 2018), that is, the energy difference between the in-plane (E_{in}) and out-of-plane (E_{out}) of $MnSi_2N_4$. For the strain-free monolayer $MnSi_2N_4$, the MAE is $-345 \mu eV/Mn$ atom, indicating that the easy axis of $MnSi_2N_4$ prefers in-plane and the spin of the Mn atoms is arranged parallel to the basal plane. The MAE of monolayer $MnSi_2N_4$ is mainly derived from Mn atoms since Mn atoms have relatively stronger spin-orbit coupling than other atoms. The MAE is depicted as a function of strain in Figure 7B. When the structure is compressed, this value fluctuates around $-350 \mu eV/Mn$, hence the effect of compressive strain on MAE is not obvious. While MAE increases significantly with increasing tensile strain. MAE changes from $-345 \mu eV/Mn$ to $-290 \mu eV/Mn$ under the 5% tensile strain.

Conclusion

The electronic and magnetic properties of monolayer $MnSi_2N_4$ are explored based on first-principles calculations. Monolayer $MnSi_2N_4$ is an intrinsic antiferromagnetic semiconductor with a small indirect band gap (0.26 eV). The $MnSi_2N_4$ has strong antiferromagnetic coupling along with strong in-plane magnetocrystalline anisotropy energy

($-345 \mu eV/Mn$). Furthermore, the $MnSi_2N_4$ monolayer exhibits half-metallic properties with a metallic spin-up state and a semiconducting spin-down state. The effect of biaxial strain on magnetism is also investigated. The magnetic exchange parameter J and MAE increase with biaxial tensile strain. The tunable magnetic properties may enrich the 2D antiferromagnets community and stimulate potential applications in spintronic devices.

Data availability statement

The original contributions presented in the study are included in the article/Supplementary Material, further inquiries can be directed to the corresponding author.

Author contributions

DC and ZJ: Conceptualization, methodology, software; JY and J-JH: Investigation, Formal analysis, Visualization; JZ and YG: Formal analysis, Data Curation; DC and YT: Writing—original draft preparation; JY: Supervision, Writing—review and editing.

Funding

Conflict of interest

The authors declare that the research was conducted in the absence of any commercial or financial relationships that could be construed as a potential conflict of interest.

Publisher's note

All claims expressed in this article are solely those of the authors and do not necessarily represent those of their affiliated organizations, or those of the publisher, the editors and the reviewers. Any product that may be evaluated in this article, or claim that may be made by its manufacturer, is not guaranteed or endorsed by the publisher.

References

Bafekry, A., Faraji, M., Stampfl, C., Abdolhosseini Sarsari, I., Abdollahzadeh Ziabari, A., Hieu, N. N., et al. (2021). Band-gap engineering, magnetic behavior and Dirac-semimetal character in the MoSi$_2$N$_4$ nanoribbon with armchair and zigzag edges. *J. Phys. D. Appl. Phys.* 55 (3), 035301. doi:10.1088/1361-6463/ac2cab

Blöchl, P. E. (1994). Projector augmented-wave method. *Phys. Rev. B* 50 (24), 17953–17979. doi:10.1103/PhysRevB.50.17953

Bonilla, M., Kolekar, S., Ma, Y., Diaz, H. C., Kalappattil, V., Das, R., et al. (2018). Strong room-temperature ferromagnetism in VSe$_2$ monolayers on van der Waals substrates. *Nat. Nanotechnol.* 13, 289–293. doi:10.1038/s41565-018-0063-9

Canton-Vitoria, R., Sayed-Ahmad-Baraza, Y., Humbert, B., Arenal, R., Ewels, C., and Tagmatarchis, N. (2020). Pyrene coating transition metal disulfides as protection from photooxidation and environmental aging. *Nanomaterials* 10 (2), 363. doi:10.3390/nano10020363

Dudarev, S. L., Botton, G. A., Savrasov, S. Y., Humphreys, C. J., and Sutton, A. P. (1998). Electron-energy-loss spectra and the structural stability of nickel oxide: An LSDA+ U study. *Phys. Rev. B* 57 (3), 1505–1509. doi:10.1103/PhysRevB.57.1505

Gong, C., Li, L., Li, Z., Ji, H., Stern, A., Xia, Y., et al. (2017). Discovery of intrinsic ferromagnetism in two-dimensional van der Waals crystals. *Nature* 546 (7657), 265–269. doi:10.1038/nature22060

Goodenough, J. B. (1955). Theory of the role of covalence in the perovskite-type manganites [La, M (II)] MnO$_3$. *Phys. Rev.* 100 (2), 564–573. doi:10.1103/PhysRev.100.564

Huang, B., Clark, G., Navarro-Moratalla, E., Klein, D. R., Cheng, R., Seyler, K. L., et al. (2017). Layer-dependent ferromagnetism in a van der Waals crystal down to the monolayer limit. *Nature* 546 (7657), 270–273. doi:10.1038/nature22391

Hung, N. T., Nugraha, A. R. T., and Saito, R. (2018). Two-dimensional MoS$_2$ electromechanical actuators. *J. Phys. D. Appl. Phys.* 51 (7), 075306. doi:10.1088/1361-6463/aaa68f

Jain, A., Hautier, G., Moore, C. J., Ping Ong, S., Fischer, C. C., Mueller, T., et al. (2011). A high-throughput infrastructure for density functional theory calculations. *Comput. Mat. Sci.* 50 (8), 2295–2310. doi:10.1016/j.commatsci.2011.02.023

Kan, M., Zhou, J., Sun, Q., Kawazoe, Y., and Jena, P. (2013). The intrinsic ferromagnetism in a MnO2 monolayer. *J. Phys. Chem. Lett.* 4 (20), 3382–3386. doi:10.1021/jz4017848

Kanamori, J. (1959). Superexchange interaction and symmetry properties of electron orbitals. *J. Phys. Chem. Solids* 10 (2-3), 87–98. doi:10.1016/0022-3697(59)90061-7

Kresse, G., and Furthmüller, J. (1996). Efficient iterative schemes for *ab initio* total-energy calculations using a plane-wave basis set. *Phys. Rev. B* 54 (16), 11169–11186. doi:10.1103/PhysRevB.54.11169

Kresse, G., and Joubert, D. (1999). From ultrasoft pseudopotentials to the projector augmented-wave method. *Phys. Rev. B* 59 (3), 1758–1775. doi:10.1103/PhysRevB.59.1758

Lee, J. U., Lee, S., Ryoo, J. H., Kang, S., Kim, T. Y., Kim, P., et al. (2016). Ising-type magnetic ordering in atomically thin FePS$_3$. *Nano Lett.* 16 (12), 7433–7438. doi:10.1021/acs.nanolett.6b03052

Ling, C., and Mizuno, F. (2012). Capture lithium in αMnO$_2$: Insights from first principles. *Chem. Mat.* 24 (20), 3943–3951. doi:10.1021/cm302347j

Liu, L., Feng, Y. P., and Shen, Z. X. (2003). Structural and electronic properties of h-BN. *Phys. Rev. B* 68 (10), 104102. doi:10.1103/PhysRevB.68.104102

Mermin, N. D., and Wagner, H. (1966). Absence of ferromagnetism or antiferromagnetism in one-or two-dimensional isotropic Heisenberg models. *Phys. Rev. Lett.* 17 (22), 1133–1136. doi:10.1103/PhysRevLett.17.1133

Novoselov, K. S., Geim, A. K., Morozov, S. V., Jiang, D., Zhang, Y., Dubonos, S. V., et al. (2004). Electric field effect in atomically thin carbon films. *Science* 306 (5696), 666–669. doi:10.1126/science.1102896

O'Hara, D. J., Zhu, T., Trout, A. H., Ahmed, A. S., Luo, Y. K., Lee, C. H., et al. (2018). Room temperature intrinsic ferromagnetism in epitaxial manganese selenide films in the monolayer limit. *Nano Lett.* 18 (5), 3125–3131. doi:10.1021/acs.nanolett.8b00683

Perdew, J. P., Burke, K., and Ernzerhof, M. (1996). Generalized gradient approximation made simple. *Phys. Rev. Lett.* 77 (18), 3865–3868. doi:10.1103/PhysRevLett.77.3865

Sheng, X. L., Chen, C., Liu, H., Chen, Z., Yu, Z. M., Zhao, Y., et al. (2019). Two-dimensional second-order topological insulator in graphdiyne. *Phys. Rev. Lett.* 123 (25), 256402. doi:10.1103/PhysRevLett.123.256402

Song, T. C., Cai, X., Tu, M. W. Y., Zhang, X., Huang, B., Wilson, N. P., et al. (2018). Giant tunneling magnetoresistance in spin-filter van der Waals heterostructures. *Science* 360, 1214–1218. doi:10.1126/science.aar4851

Togo, A., and Tanaka, I. (2015). First principles phonon calculations in materials science. *Scr. Mat.* 108, 1–5. doi:10.1016/j.scriptamat.2015.07.021

Wang, L., Maxisch, T., and Ceder, G. (2006). Oxidation energies of transition metal oxides within the GGA+U framework. *Phys. Rev. B* 73 (19), 195107. doi:10.1103/PhysRevB.73.195107

Webster, L., and Yan, J. A. (2018). Strain-tunable magnetic anisotropy in monolayer CrCl3, CrBr3, and CrI3. *Phys. Rev. B* 98 (14), 144411. doi:10.1103/PhysRevB.98.144411

Xian, J. J., Wang, C., Nie, J. H., Li, R., Han, M., Lin, J., et al. (2022). Spin mapping of intralayer antiferromagnetism and field-induced spin reorientation in monolayer CrTe$_2$. *Nat. Commun.* 13, 257. doi:10.1038/s41467-021-27834-z

Yuan, J., Wei, Q., Sun, M., Yan, X., Cai, Y., Shen, L., et al. (2022). Protected valley states and generation of valley-and spin-polarized current in monolayer MA$_2$Z$_4$. *Phys. Rev. B* 105 (19), 195151. doi:10.1103/PhysRevB.105.195151